THE JOURNAL OF PHYSICAL CHEMISTRY B

ARTICLE

pubs.acs.org/JPCB

Molecular Simulation of Diffusion of Hydrogen, Carbon Monoxide, and Water in Heavy *n*-Alkanes

Zoi A. Makrodimitri,[†] Dominik J. M. Unruh,[‡] and Ioannis G. Economou*[,†,§]

[†]Molecular Thermodynamics and Modelling of Materials Laboratory, Institute of Physical Chemistry, National Center for Scientific Research "Demokritos", GR-153 10 Aghia Paraskevi Attikis, Greece

[‡]Shell Global Solutions International BV, PO Box 38000, 1030 BN Amsterdam, The Netherlands

[§]Department of Chemical Engineering, The Petroleum Institute, PO Box 2533, Abu Dhabi, United Arab Emirates

ABSTRACT: The self-diffusion and mutual diffusion coefficients of hydrogen (H_2), carbon monoxide (CO), and water (H_2O) in *n*-alkanes were studied by molecular dynamics simulation. *n*-Alkane molecules were modeled based on the TraPPE united atom force field. NPT molecular dynamics (MD) simulations were performed for *n*-C_{12} to *n*-C_{96} at different temperature and pressure values to validate the accuracy of the force field. In all cases, good agreement was obtained between literature experimental data and model predictions for the density and structure properties of the *n*-alkanes. Subsequently, the self-diffusion coefficient of the three light components in the various *n*-alkanes was calculated at different temperatures. Model predictions were in very good agreement with limited experimental data. Furthermore, the Maxwell−Stefan diffusion coefficients of H_2 and CO in two *n*-alkanes, namely *n*-C_{12} and *n*-C_{28}, were calculated based on long MD NVT simulations for different solute concentrations in the *n*-alkanes. Finally, the Fick diffusion coefficient of the components was calculated as a product of the Maxwell−Stefan diffusion coefficient and a thermodynamic factor. The latter was estimated from the statistical associating fluid theory (SAFT). The Fick diffusion coefficient was found to be higher than the Maxwell−Stefan diffusion coefficient for H_2 and CO in *n*-C_{28}. The empirical Darken equation was used to estimate the Maxwell−Stefan diffusion coefficient, and calculations were found to be in good agreement with simulation results.

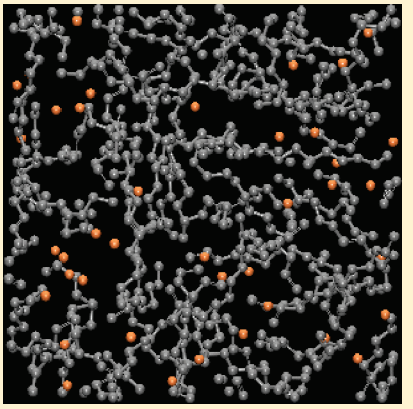

1. INTRODUCTION

Diffusion coefficient, density, and viscosity are important thermophysical properties that control mass-transfer phenomena and are used for equipment design for mass-transfer operations. Typically, these properties are measured experimentally. Often though, experimental measurements are cumbersome and/or expensive. This is true, for example, for the measurement of the diffusion coefficient of solutes in liquid solvents in the low concentration limit and at conditions far from ambient. In such cases, theoretical models or accurate computational approaches are preferred.

Significant research has been devoted to the estimation of the diffusion coefficient in mixtures using different theoretical approaches. For example, the diffusion coefficients of various solutes in hydrocarbons in the dilute regime have been calculated based on the modified Stokes−Einstein relation,[1] the penetration length model,[2] and generalized free volume theories,[3] and empirical correlations have been proposed based on the size and shape of diffusing molecules.

Although these theoretical approaches are very useful for the estimation of diffusion coefficient in multicomponent systems, they are not always easy to apply and are, in general, only valid in dilute or semidilute regimes. Molecular simulation represents a reliable alternative tool for the estimation of diffusion coefficients thanks to the tremendous increase of computing power and the development of accurate molecular models and advanced simulation methods.[4−7]

The diffusion coefficient of hydrogen (H_2), carbon monoxide (CO), and water (H_2O) in *n*-alkanes is needed for the evaluation of mass transport in high-temperature industrial processes such as hydrogenation, hydrotreating, Fischer−Tropsch synthesis, coal liquefaction, etc. In particular, the gas to liquid (GTL) process is a very promising technology for the production of high-value fuels (heavy *n*-alkanes, etc.) and is based on Fischer−Tropsch synthesis. The key reaction in this process involves conversion of a mixture of H_2 and CO into liquid hydrocarbons according to the general chemical reaction

$$nCO + (2n+1)H_2 \rightarrow C_nH_{2n+2} + nH_2O \qquad (1)$$

In eq 1, it is assumed for simplicity that only *n*-alkanes of variable length are produced, although additional hydrocarbons may be generated. Depending on the process conditions,

Received: July 8, 2010
Revised: November 17, 2010
Published: January 21, 2011

dx.doi.org/10.1021/jp1063269 | *J. Phys. Chem. B* 2011, 115, 1429–1439

Table 1. Atomistic UA Force Field for *n*-Alkanes, H_2, CO, and H_2O Molecules

type of interaction		potential function and parameters	
bond stretching		$V_{stretching}(l) = {}^1/_2 k_l (l - l_0)^2$	
	bond	k_l (kcal/mol/Å^2)	l_0 (Å)
	C−C	192.0	1.54
	H−O (water)	824.5	1.00
bond bending		$V_{bending}(\theta) = {}^1/_2 k_\theta (\theta - \theta_0)^2$	
	bond angle	k_θ (kcal/mol deg^2)	θ_0 (deg)
	C−C−C	0.038	114.00
	H−O−H (water)	0.028	109.47
dihedral angle		$V_{dihedral} = \sum_{i=1}^{3} a_i[1 + (-1)^{i+1} \cos(i\varphi)]$	
		C−C−C−C a_1/k_B = 355.03 K, a_2/k_B = −68.19 K, a_3/k_B = 791.32 K	
nonbonded Lennard-Jones		$V_{LJ} r_{ij} = 4\varepsilon_{ij}[(\sigma_{ij}/r_{ij})^{12} - (\sigma_{ij}/r_{ij})^6]$	
		σ (Å)	ε (kcal/mol)
	CH_2	3.950	0.091
	CH_3	3.750	0.195
	O (water)	3.166	0.155
	H_2 (hydrogen)	2.970	0.066
	CO	3.920	0.065
nonbonded electrostatic		$V_q r_{ij} = ((q_i q_j)/(4\pi\varepsilon_0))((1/r_{ij} + ((\varepsilon_s - 1)r_{ij}^2)/((2\varepsilon_s + 1)r_c^3)))$	
		H (water)	O (water)
	q (esu)	0.4238	−0.8476

n may vary widely and assume a broad range of values, from below 10 up to close or even above 100. For the accurate modeling of the process, the diffusion coefficient of H_2, CO, and H_2O in the *n*-alkane mixture should be known as a function of temperature and pressure. Typical range of conditions includes temperatures from 450 to 540 K and pressures from 2 to 8 MPa.

In this work, molecular dynamics (MD) simulations were performed in order to calculate the diffusion coefficient of H_2, CO, and H_2O in various *n*-alkanes, namely from *n*-C_{12} up to *n*-C_{96}, at high-temperature and -pressure conditions. For *n*-alkanes, an accurate united atom (UA) force field was used.[8] H_2 and CO were modeled as Lennard-Jones spheres whereas for H_2O the popular extended simplified point charge (SPC/E) model was used.[9] Long NVT simulation runs, on the order of 30 ns, were performed in order to obtain reliable results. Limited experimental data[10−12] for the diffusion coefficient of the light components in *n*-C_{12}, *n*-C_{16}, and *n*-C_{28} were used for the evaluation of simulation results. Furthermore, the Maxwell−Stefan diffusion coefficient of H_2 and CO in *n*-C_{12} and *n*-C_{28} was calculated for different solute concentrations and used subsequently for the calculation of the Fick diffusion coefficient. In the latter calculation, the nonideal thermodynamic effect should be taken into account. It can be calculated either based on molecular simulation or based on a macroscopic model, such as an equation of state (EoS). In this work, the statistical associating fluid theory (SAFT) was used that provides a good compromise between accuracy and simplicity.[13] Since experimental data are not available for Maxwell−Stefan and Fick diffusion coefficients, simulation results were compared against predictions from the empirical Darken's correlation.

2. ATOMISTIC FORCE FIELD AND SIMULATION DETAILS

In this work, a UA representation was used to model the *n*-alkane molecules. In particular, the transferable potential for phase equilibria (TraPPE)[8] was employed. TraPPE has been shown to be very accurate for the thermodynamic properties of *n*-alkanes in the pure state and in mixtures over a wide range of conditions, including the critical point and, of course, the range of temperature and pressure values of importance to the current project. According to this force field, the potential energy function is written as the sum of contributions due to bond stretching, bond angle bending, dihedral angle torsion, and nonbonded intra- and intermolecular interactions:

$$\begin{aligned} V_{total}(\mathbf{r}_1, \ldots, \mathbf{r}_N) &= V_{stretching} + V_{bending} + V_{torsion} + V_{nonbonded} \\ &= \sum_{\text{all bonds}} \frac{k_{l_i}}{2}(l_i - l_{i,0})^2 + \sum_{\text{all bond angles}} \frac{k_{\theta_i}}{2}(\theta_i - \theta_{i,0})^2 \\ &\quad + \sum_{\text{all dihedral angles}} \sum_{i=1}^{3} a_i \left[1 + (-1)^{i+1} \cos(i\phi)\right] \\ &\quad + \sum_{\text{all pairs}} \left(4\varepsilon_{ij} \left[\left(\frac{\sigma_{ij}}{r_{ij}}\right)^{12} - \left(\frac{\sigma_{ij}}{r_{ij}}\right)^{6} \right] + \frac{q_i q_j}{4\pi\varepsilon_0} \left(\frac{1}{r_{ij}} + \frac{(\varepsilon_s - 1) r_{ij}^2}{(2\varepsilon_s + 1) r_c^3} \right) \right) \end{aligned} \quad (2)$$

where l_i, θ_i, and ϕ_i denote bond length, bond angle, and dihedral angle, respectively, r_{ij} is the distance between interaction sites *i* and *j*, and q_i is the partial charge on site *i*. Subscript 0 denotes the parameter value at equilibrium. Flexible bonds are used and the potential energy of each bond is evaluated by using a simple harmonic potential (first term on the rhs of eq 2). Similarly, bond-angle fluctuations around the equilibrium angle are subject to harmonic fluctuations (second term

dx.doi.org/10.1021/jp1063269 |J. Phys. Chem. B 2011, 115, 1429–1439

Table 2. Details of the Simulated Pure *n*-Alkane Systems

n- alkane	no. of chains	temperature (K)	pressure (MPa)
n-C_{12}	60	443, 473, 513	1.40, 3.40
n-C_{16}	60	443, 473, 513	1.40, 3.40
n-C_{28}	34	443, 473, 495	1.35, 3.40
n-C_{48}	20	443, 473	3.40
n-C_{64}	15	443, 473	3.40
n-C_{96}	10	443, 473	3.40

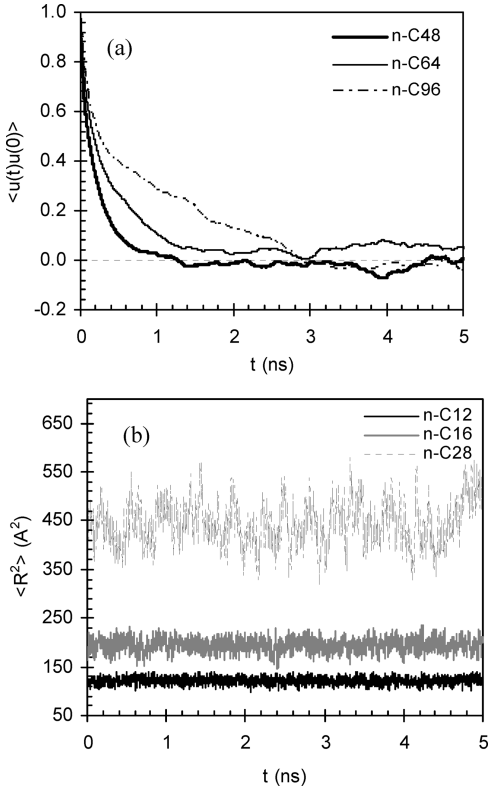

Figure 1. (a) Time decay of the autocorrelation function of the chain end-to-end unit vector, $\langle \mathbf{u}(t)\cdot\mathbf{u}(0)\rangle$, and (b) evolution of the instantaneous value of the chain end-to-end distance, $\langle R^2\rangle$, with time as obtained from the NPT MD simulations at 443 K and 3.4 MPa.

on the rhs of eq 2). The dihedral angle potential is described by a Fourier cosine expansion (third term on the rhs of eq 2). In eq 2, q_i and q_j are the partial charges of interaction sites i and j, ε_s is the dielectric constant of solvent, ε_0 is the dielectric permittivity of vacuum (equal to $8.854\,19 \times 10^{-12}$ C^2 J^{-1} m^{-1}), and r_c is the cutoff distance for the electrostatic interactions. Standard Lorentz−Berthelot combining rules are used to describe nonbonded Lennard-Jones interactions between sites of different type:

$$\varepsilon_{ij} = \sqrt{\varepsilon_{ii}\varepsilon_{jj}} \quad \text{and} \quad \sigma_{ij} = \frac{\sigma_{ii}+\sigma_{jj}}{2} \qquad (3)$$

For the light molecules (H_2, CO and H_2O), the following models were used:

- *Hydrogen*: Ferrando and Ungerer[14] examined recently various force fields for H_2 (Hirschfelder et al.,[15] corresponding state,[16] Darkrim et al.,[17] and Cracknell[18]) with respect to their accuracy for pure H_2 compressibility and for H_2−hydrocarbon phase equilibria. It was found that the Hirschfelder et al. model is more accurate for pure H_2 compressibility while the Darkrim et al. model is preferable for the prediction of H_2−hydrocarbon phase equilibria data. The latter model consists of a Lennard-Jones sphere and three partial charges which make it significantly more computationally demanding than the former one that consists of a Lennard-Jones sphere only. Consequently in this work, the Hirschfelder et al. model was used for H_2.
- *Carbon monoxide*: CO molecules were also modeled as Lennard-Jones spheres with parameters proposed by Hirschfelder et al.[15]
- *Water*: The SPC/E model was used that assumes a Lennard-Jones site on the oxygen atom and three charges on the oxygen and hydrogen atoms.[9] This force field provides a good compromise between simplicity and accuracy.

Table 3. Experimental, Calculated, and Group Contribution Values for the Melt Density of *n*-Alkanes

			density (g/cm³)		
n-alkane	*T* (K)	*P* (MPa)	expt	NPT simulation	% dev
n-C_{12}	443	3.40	0.640	0.645 ± 0.002	0.8
n-C_{12}	473	3.40	0.617	0.619 ± 0.002	0.3
n-C_{12}	513	1.40	0.575	0.578 ± 0.002	0.5
n-C_{16}	443	3.40	0.668	0.673 ± 0.003	0.7
n-C_{16}	473	3.40	0.643	0.650 ± 0.002	1.0
n-C_{16}	513	1.40	0.616	0.619 ± 0.002	0.5
n-C_{28}	443	1.35	0.710	0.715 ± 0.004	0.7
n-C_{28}	473	3.40	0.696	0.701 ± 0.004	0.7
n-C_{28}	495	1.35	0.675	0.680 ± 0.005	0.7
			density (g/cm³)		
			group contribn		
n-alkane	*T* (K)	*P* (MPa)	method	NPT simulation	% dev
n-C_{48}	443	3.40	0.734	0.742 ± 0.001	1.1
n-C_{48}	473	3.40	0.718	0.729 ± 0.002	1.5
n-C_{64}	443	3.40	0.742	0.752 ± 0.001	1.3
n-C_{64}	473	3.40	0.726	0.739 ± 0.002	1.8
n-C_{96}	443	3.40	0.750	0.761 ± 0.002	1.5
n-C_{96}	473	3.40	0.734	0.747 ± 0.003	1.8

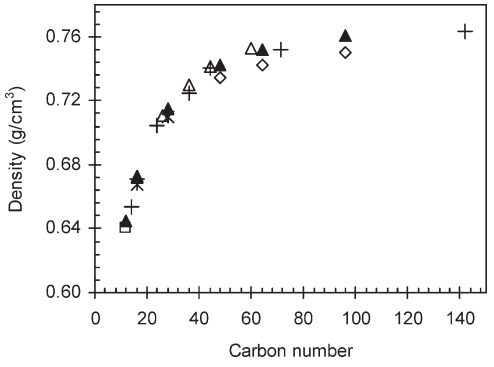

Figure 2. Melt densities of *n*-alkanes as a function of carbon number at 443 K: experimental data (open triangles from ref 29; crosses from ref 30; open square from ref 25; and stars from ref 26), group contribution method calculations (open diamonds from ref 27), and MD predictions (filled points).

dx.doi.org/10.1021/jp1063269 |J. Phys. Chem. B 2011, 115, 1429–1439

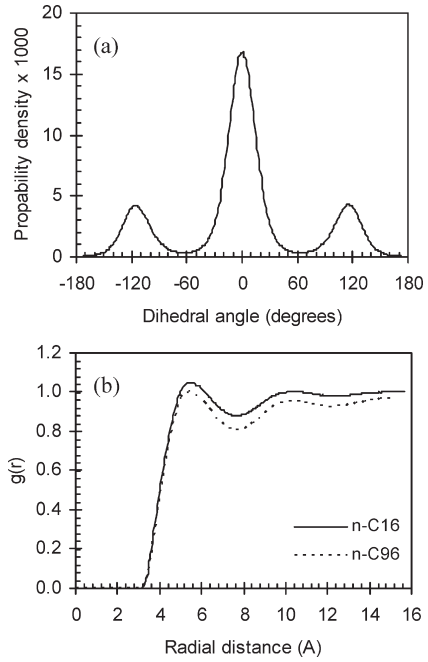

Figure 3. (a) Distribution of C−C−C−C dihedral angle of n-C_{16} and (b) total intermolecular pair distribution function for the n-C_{16} and n-C_{96} at 443 K and 3.4 MPa obtained from NPT MD simulation.

Table 4. Mean Squared End-to-End Distance, $\langle R^2 \rangle$, Mean Squared Radius of Gyration, $\langle R_g{}^2 \rangle$, and Their Ratio for Various Chain Lengths of n-Alkanes at 473 K and 3.4 MPa

n-alkane	$\langle R^2 \rangle$ (Å^2)	$\langle R_g{}^2 \rangle$ (Å^2)	$\langle R^2 \rangle / \langle R_g{}^2 \rangle$
n-C_{12}	119.2 ± 0.2	14.3 ± 0.1	8.33 ± 0.05
n-C_{16}	190.7 ± 0.7	23 ± 1	8.3 ± 0.4
n-C_{28}	425 ± 5	54.3 ± 0.4	7.8 ± 0.1
n-C_{48}	839 ± 25	115 ± 2	7.2 ± 0.3
n-C_{64}	1136 ± 97	163 ± 8	6.9 ± 0.7
n-C_{96}	2054 ± 163	302 ± 15	6.8 ± 0.6

The parameters for the force fields used for n-alkane, H_2, CO, and H_2O molecules are listed in Table 1.

MD simulations were performed at the isobaric−isothermal (NPT) ensemble using Nosé and Klein extended method[19] and at the canonical (NVT) ensemble. In NPT simulations, an integration time step of 0.5 fs and the fifth-order Gear predictor−corrector scheme[20] was used to integrate the equations of motion in Cartesian coordinates. The duration of the simulation runs was up to 10 ns. Specific details of the simulated systems are reported in Table 2. The initial configurations were obtained using the Cerius^2 software package of Accelrys Inc. n-Alkane chains were built in an amorphous cell using periodic boundary conditions. These initial configurations were subjected to molecular mechanics. Energy minimization took place in two stages. First, the steepest descent method was used with a maximum number of iterations equal to 100 followed by the conjugate gradient method with a maximum number of iterations up to 10 000.

In all simulations, periodic boundary conditions were applied to the simulation box. A Verlet neighbor list and a truncated Lennard-Jones and electrostatic potential were used to speed up calculations of interactions between molecules. In this work, the

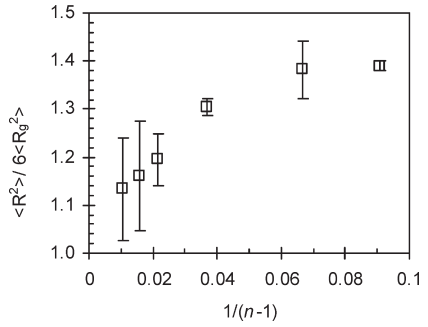

Figure 4. NPT MD predictions for the mean squared end-to-end distance $\langle R^2 \rangle$ divided by the mean squared radius of gyration $\langle R_g{}^2 \rangle$ as a function of n-alkane chain length at 473 K and 3.4 MPa. For a Gaussian chain, $\langle R^2 \rangle / (6\langle R_g{}^2 \rangle) = 1$.

Table 5. Details of the Simulated n-Alkane−Solute Systems

n- alkane	no. of chains	no. of H_2 molecules	no. of CO molecules	no. of H_2O molecules
n-C_{12}	60	10	10	3
n-C_{16}	60	10	10	3
n-C_{28}	30	10	10	1
n-C_{48}	20	10	10	1
n-C_{64}	15	10	10	1
n-C_{96}	10	10	10	1

Lennard-Jones potential tail beyond $r = 1.45\sigma$ was substituted by a fifth-order polynomial, whose value beyond $r = 2.33\sigma$ is equal to zero.[21] This approach has been used extensively for the past 25 years for the molecular simulation of a wide range of fluids that includes gases, liquids, polymers, etc. For electrostatic interactions, the cutoff distance, r_c, was equal to 13.5 Å, a value which is smaller than half the box edge length. The instantaneous pressure P_{int} was calculated during the simulation according to the molecular virial expression proposed by Theodorou et al.[22] The "tail" contributions to the internal energy and to the pressure were taken into account.[23]

Moreover, long NVT MD simulations at the experimental density and on the order of 30 ns were performed for the estimation of the self-diffusion coefficient of light gases in n-alkanes. In these simulations, an increased time step of 2 fs was used and the equations of motion were integrated using the velocity Verlet algorithm.[23] In all cases, to maintain the temperature fixed at its prescribed value, the Berendsen thermostat[24] was used with coupling constant equal to 0.1 ps. Simulations were performed in machines based on Intel Xeon CPU 2.8 GHz processor. To decrease the uncertainty in D calculations, four initially different structures of each n-alkane were examined.

3. RESULTS AND DISCUSSION

3.1. System Equilibration. In Figure 1a, NPT MD predictions are shown for the time decay of the autocorrelation function $\langle \mathbf{u}(t) \cdot \mathbf{u}(0) \rangle$ for the unit vector $\mathbf{u}$ that is directed along the chain end-to-end vector. Calculations are presented for n-C_{48}, n-C_{64}, and n-C_{96} pure liquids at 443 K and 3.4 MPa. In all cases, the function $\langle \mathbf{u}(t) \cdot \mathbf{u}(0) \rangle$ is seen to decay to zero after a few nanoseconds. The decay depends strongly on the n-alkane size and becomes slower for the larger n-alkane. In Figure 1b, the change of the mean squared chain end-to-end

dx.doi.org/10.1021/jp1063269 |J. Phys. Chem. B 2011, 115, 1429–1439

Table 6. Experimental and Calculated Self-Diffusion Coefficients, *D*, of Solutes in *n*-Alkanes

	self-diffusion coefficient ($D \times 10^9$ m^2/s)				
	H_2		CO		H_2O
T (K)	experiment	NVT simulation	experiment	NVT simulation	NVT simulation
			Solvent: *n*-C_{12}		
443	41.0 ± 1.0	38 ± 3	17.6 ± 0.2	19.5 ± 0.5	22.4 ± 0.4
473	57.6	39 ± 2	22.5	22 ± 1	27 ± 1
513	78.0 ± 4.8	55 ± 5	27.0 ± 0.7	28 ± 1	35 ± 4
			Solvent: *n*-C_{16}		
443	35.2 ± 2.5	35 ± 3	13.1 ± 0.5	15.0 ± 0.2	20 ± 1
473	40.7	37 ± 1	16.8	19 ± 1	25 ± 1
513	51.2 ± 2.5	50 ± 4	22.5 ± 0.6	25.2 ± 0.3	31.2 ± 0.7
			Solvent: *n*-C_{28}		
443	27	31 ± 4	9.6	12.1 ± 0.1	17 ± 3
473	34.4	34 ± 1	12.5	14.7 ± 0.7	22 ± 4
495	41	39 ± 1	15.7 ± 0.5	20.3 ± 0.8	22.6 ± 0.7
			Solvent: *n*-C_{48}		
443	–	26 ± 3	–	9.7 ± 0.3	12.0 ± 0.3
473	–	30 ± 1	–	12.5 ± 0.4	19 ± 3
			Solvent: *n*-C_{64}		
443	–	23 ± 1	–	8 ± 2	11 ± 2
473	–	28 ± 2	–	10.5 ± 0.3	18 ± 2
			Solvent: *n*-C_{96}		
443	–	22 ± 1	–	7 ± 1	9 ± 2
473	–	25 ± 2	–	9.7 ± 0.4	14 ± 1

distance, $\langle R^2 \rangle$, for three *n*-alkane liquids (*n*-C_{12}, *n*-C_{16}, and *n*-C_{28}) with time is examined. $\langle R^2 \rangle$ assumes a relatively constant value which is characteristic of a well-equilibrated system. Similar behavior was observed for all systems studied at all temperatures.

3.2. Thermodynamic Properties. MD simulations were performed for various pure *n*-alkanes, including: *n*-C_{12}, *n*-C_{16}, *n*-C_{28}, *n*-C_{48}, *n*-C_{64}, and *n*-C_{96} at various temperature and pressure conditions. In Table 3, experimental density values from NIST database[25] for *n*-C_{12}, from DIPPR database[26] and from Rodden et al.[10] for *n*-C_{16} and *n*-C_{28}, density values obtained from the group contribution method of Elbro et al.[27,28] for *n*-C_{48} up to *n*-C_{96}, and simulated melt density for all six *n*-alkanes are presented. For the smaller *n*-alkanes, *n*-C_{12} up to *n*-C_{28}, the maximum deviation between the experimental and the measured values is less than 1%. For the larger *n*-alkanes, comparison of MD results with predictions from the group contribution method of Elbro et al.[28] reveals a deviation higher than 1%. We believe that this increased deviation should be partially attributed to the inaccuracy of the group contribution method.

In Figure 2, MD density predictions at 443 K and 3.4 MPa are shown together with experimental data[29,30] for *n*-C_{14} up to *n*-C_{142}. A sharp density increase with the carbon number is observed for low and intermediate molecular weights. For *n*-alkanes higher than approximately *n*-C_{60}, density approaches a constant value. Overall, the agreement between experimental data and MD predictions is very good in all cases. Notably, group contribution predictions are systematically lower than experimental data and NPT MD predictions.

Overall, the calculations presented here confirm earlier studies regarding the accuracy of TraPPE force field for the prediction of thermodynamic properties of long *n*-alkanes. The accuracy of the force field regarding transport properties has not been fully evaluated, yet, and so calculations presented below provide an important contribution toward this end.

3.3. Structural Properties. A critical test for the validation of the TraPPE force field used for the *n*-alkanes refers to its accuracy in reproducing the structural properties of the *n*-alkane melt as quantified by the distributions of bond lengths, bending angles, and dihedral angles and the total radial pair distribution function. Simulation results for the C−C−C−C dihedral angle distribution of *n*-C_{16} are shown in Figure 3a. The same distribution was also found for the higher *n*-alkanes. This means that the dihedral angle distribution is not influenced by the molecular weight of the *n*-alkane. The distribution shows a clear preference for the trans state (at 0°) with local maxima in gauche$^+$ (at 120°) and gauche$^-$ (at −120°) conformations, in agreement with MD calculations for a series of linear polymethylene chains reported by Mattice and co-workers.[31] The percentage of trans state conformation is about 4 times higher than that of gauche state. The height of the three peaks is in agreement with the molecular simulation predictions of Zervopoulou et al. for pure *n*-C_{78}.[32]

In Figure 3b, total intermolecular pair distribution function predictions are shown for *n*-C_{16} and *n*-C_{96} at 443 K and 3.4 MPa.

dx.doi.org/10.1021/jp1063269 |*J. Phys. Chem. B* 2011, 115, 1429–1439

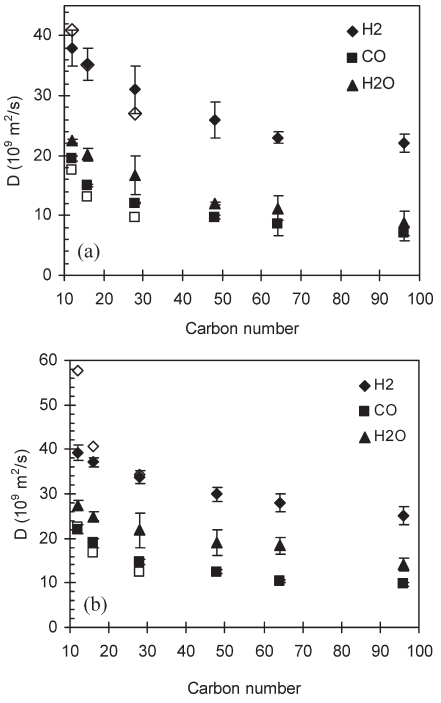

Figure 5. Self-diffusion coefficient of H_2, CO and H_2O in *n*-alkanes as a function of carbon number at (a) 443 K and (b) 473 K. Open symbols are experimental data[10,11] and solid symbols are NVT MD predictions.

Table 7. Pure Component Parameters Used in SAFT EoS

	n-C_{12}	*n*-C_{28}	H_2	CO
m	8.730	19.287	1.000	0.931
v^{00} (mL/mol)	11.884	12.000	13.625	221.574
u^0/k (K)	208.31	209.96	39.17	136.30
ε/k (K)	10	10	0	4

For both *n*-alkanes, simulation results exhibit two rather broad peaks at ~5 and 10 Å, characteristic of local packing in *n*-alkanes.[33] As the size of the *n*-alkane chain increases, the "correlation hole effect" is more pronounced. This means that at distances smaller than the mean squared radius of gyration of *n*-alkane, $g(r)$ is below 1, because the cloud of segments belonging to the reference chain excludes segments of other chains from approaching the reference segment. This behavior has also been observed for high molecular weight polyethylene melt systems by Mavrantzas et al.[34] Furthermore, an increase in the chain length results in a small shift of the first peak position to lower distances, due to an increase of the density, which results to closer packing.

Results for the mean squared end-to-end distance $\langle R^2 \rangle$ as well as for the mean squared radius of gyration $\langle R_g^2 \rangle$ for different *n*-alkane chain lengths at 473 K and 3.4 MPa are presented in Table 4. For Gaussian chains, according to Flory's random coil hypothesis, the following equation holds:

$$\langle R^2 \rangle = 6\langle R_g^2 \rangle \tag{4}$$

MD predictions for the ratio $\langle R^2 \rangle/(6\langle R_g^2 \rangle)$ are shown in Figure 4. It is clear that, for all chain lengths examined here $(12 \leq n \leq 96)$, chains are extended and a non-Gaussian behavior is observed. As the chain length increases, the ratio decreases and approaches 1. Consequently, for this model and

Table 8. Binary Interaction Parameters Used for SAFT Mixture Calculations Fitted to Experimental Phase Equilibrium Data from the Literature

mixture	k_{ij}	ref[a]
H_2−*n*-C_{12}	0.3151	49
H_2−*n*-C_{16}	0.2518	50
H_2−*n*-C_{28}	0.4413	51
CO−*n*-C_{12}	0.1920	49
CO−*n*-C_{16}	0.2014	interpolated (refs 49 and 52)
CO−*n*-C_{28}	0.2297	52

[a] Experimental data used to fit the k_{ij} values.

temperature, the crossover to Gaussian statistics occurs for *n* significantly greater than 100. A similar result was found by Baschnagel et al.,[35] Brown et al.,[36] Modello et al.,[37] and Paul et al.[38] for liquid *n*-alkanes.

3.4. Self-Diffusion Coefficient Calculations. Long NVT MD simulations on the order of 30 ns each were performed for the calculation of the self-diffusion coefficient of solutes in *n*-alkanes. A number of solute molecules were dispersed randomly in the *n*-alkane liquid, and their displacement was monitored over time. In all cases, the mole fraction of the solute was below the solubility limit at the specific temperature and pressure. The density of the systems remained constant and equal to the experimental density of pure *n*-alkanes. Details of the simulated systems are presented in Table 5. For the smaller *n*-alkanes, *n*-C_{12} up to *n*-C_{28}, simulations were performed at three temperatures for each mixture, that is, 443, 473, and 513 K (495 K for *n*-C_{28}), while for the larger *n*-alkanes, *n*-C_{48} up to *n*-C_{96}, two temperatures were examined, that is, 443 and 473 K. The solute self-diffusion coefficient, D, is defined based on the mass current of a single target molecule and is calculated from the linear part of the mean square displacement of the centers of mass of the solute molecules according to the Einstein equation:[39]

$$D = \lim_{t \to \infty} \frac{1}{6} \frac{d}{dt} \left\langle \left| r_i(t) - r_i(0) \right|^2 \right\rangle \tag{5}$$

where $r_i(t)$ is the center-of-mass vector position of each molecule i at time t. The brackets indicate time and particle average.

In Table 6 and Figure 5, experimental data[10,11] and NVT MD predictions for the self-diffusion coefficient of the three solutes in all *n*-alkanes are shown for comparison. To decrease the uncertainty in calculations, four initially different structures of each *n*-alkane system at each temperature were examined. The statistical uncertainty reported in the simulations is the standard deviation in the calculated values for the different structures. Experimental D values for H_2 and CO in *n*-C_{12} and *n*-C_{16} at 473 K and for H_2 and CO in *n*-C_{28} at 443 and 473 K were obtained by interpolation of the experimental data proposed by Matthews et al.[11] and Rodden et al.,[10] respectively. The agreement between experimental data and simulations is very good.

The only data available in the literature for the diffusion coefficient of H_2O in *n*-alkanes are the data of Schatzberg[12] who measured experimentally the diffusion coefficient of H_2O in *n*-C_{16} in the temperature range from 298 to 318 K. By extrapolating these data to the temperature range examined in this

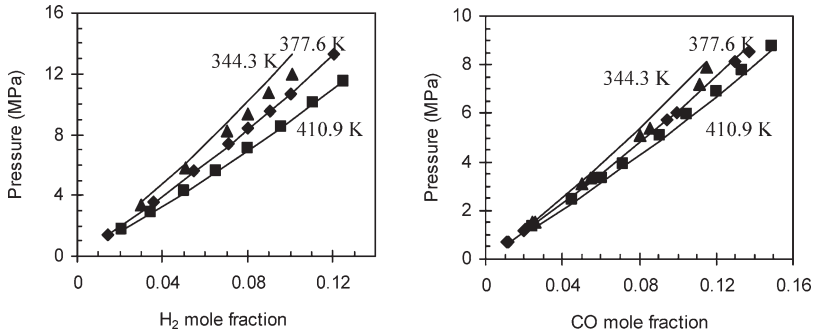

Figure 6. Experimental data[49] (points) and SAFT correlations of (left) H_2 and (right) CO solubility in n-C_{12}.

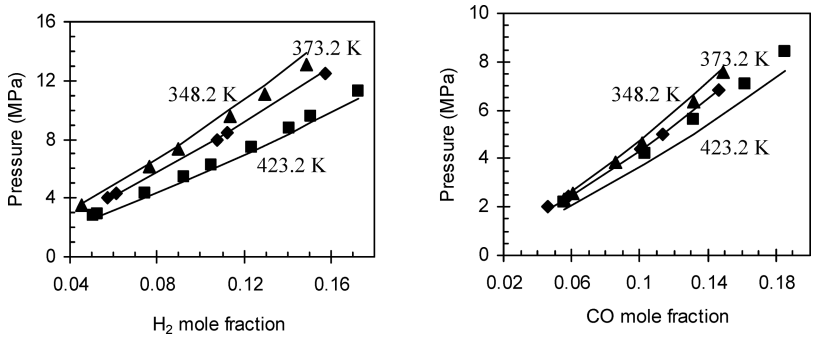

Figure 7. Experimental data[51,52] (points) and SAFT correlations of (left) H_2 and (right) CO solubility in n-C_{28}.

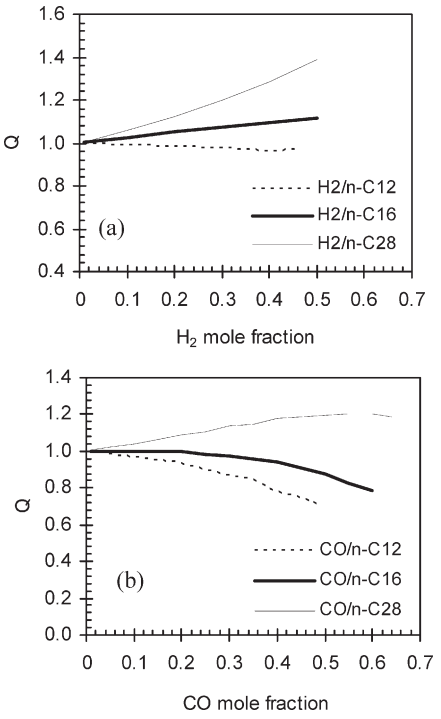

Figure 8. SAFT prediction of the thermodynamic factor Q as a function of (a) H_2 and (b) CO mole fraction in n-C_{12}, n-C_{16}, and n-C_{28} at 473 K.

work and assuming Arrhenius temperature dependence, the diffusion coefficient of H_2O in n-C_{16} is equal to 26.4×10^{-9}, 33.6×10^{-9}, and 44.3×10^{-9} m^2/s at 443, 473, and 513 K, respectively. Given the temperature range of the original experimental data, these values are in reasonable agreement with the simulated values presented here. Moreover, no experimental data were found in the literature regarding the diffusion of light components in larger n-alkanes.

3.5. Effect of Gas Composition on the Diffusion Coefficient. In a binary mixture, one may define two kinds of diffusion coefficients: self-diffusion and mutual diffusion coefficients. The self-diffusion coefficient, calculated in the previous section, describes the mobility of individual molecule in the mixture in the absence of a driving force for diffusion, and it arises due to the Brownian motion (random walk) of the molecule. The mutual diffusion coefficient is a collective property, which determines the concerted ability of species 1 to diffuse through species 2 and it relates a mass or molar flux to a driving force, such as a gradient in the concentration of the particular species. Several attempts were conducted recently to estimate the mutual diffusion coefficient in mixtures using molecular simulation methods.[7,40−46] To the best of our knowledge, apart from the work of Zabala et al.[45] who calculated the mutual diffusion coefficient of CO_2 in n-alkanes, and the work of Rousseau et al.[7,46] who estimated the mutual diffusion coefficient of CO_2, CH_4, and C_2H_6 in n-C_{10}, of CO_2 in C_2H_6, and of N_2 in n-C_5H_{12}, no other data exist in the literature concerning the mutual diffusivity of gases in hydrocarbons.

According to Fick's law and the Gibbs−Duhem equation, the mutual diffusion coefficient, D_{12}^{Fick}, can be written as a product of a thermodynamic factor, Q, and the Maxwell−Stefan diffusion coefficient, D_{12}^{MS}:[47]

$$D_{12}^{Fick} = QD_{12}^{MS} \quad (6)$$

The Maxwell−Stefan diffusion coefficient is a kinetic factor and it can be determined from the mean-square displacement of the

dx.doi.org/10.1021/jp1063269 |J. Phys. Chem. B 2011, 115, 1429–1439

Table 9. Pressure Values for the Mixture State Points Where NVT MD Simulations Were Performed at 473 K

	pressure (MPa)	
H_2 mole fraction	H_2−n-C_{12}	H_2−n-C_{28}
0.1	10	6
0.2	20	12
0.3	30	20
0.4		35
0.5		50
	pressure (MPa)	
CO mole fraction	CO−n-C_{12}	CO−n-C_{28}
0.1	6	6
0.2	12	12
0.3	20	20
0.4	30	30
0.5		40

Table 10. D^{MS} from NVT MD Simulations as a Function of Composition at 473 K

	Maxwell−Stefan diffusion coeff ($D^{MS} \times 10^9$ m^2/s)	
H_2 mole fraction	n-C_{12}	n-C_{28}
0.1	45 ± 10	34 ± 2
0.2	43 ± 6	36 ± 2
0.3	38 ± 9	30 ± 5
0.4		29 ± 4
0.5		22 ± 2
	Maxwell−Stefan diffusion coeff ($D^{MS} \times 10^9$ m^2/s)	
CO mole fraction	n-C_{12}	n-C_{28}
0.1	25 ± 3	12.3 ± 0.8
0.2	22 ± 2	12.5 ± 0.9
0.3	20 ± 2	10.9 ± 0.9
0.4	19 ± 3	9.1 ± 0.9
0.5		9 ± 1

center of mass of particles of species 1 (here the solute):[40,48]

$$D_{12}^{MS} = \frac{1}{6Nx_1x_2}\left(\frac{m_1}{m_2}x_1 + x_2\right)^2 \times \lim_{t\to\infty}\frac{d}{dt}\left\langle\left[\sum_{k=1}^{N_1} r_k(0) - \sum_{k=1}^{N_1} r_k(t)\right]^2\right\rangle \quad (7)$$

where N is the total number of particles, $x_1 = N_1/N$ and $x_2 = N_2/N$ are the mole fractions of species 1 and 2, and N_1 and N_2 are the number of particles of type 1 and 2, respectively; m_1 and m_2 are the masses of the two different types of particles and $r_k(t)$ is the position of particle k of species 1 at time t.

The Maxwell−Stefan diffusion coefficient calculated from eq 7 is subject to greater statistical noise than the self-diffusion coefficient. The reason for this is that each molecule contributes independent information to the self-diffusion coefficient at every time step, providing N_1 data points to which the self-diffusion coefficient will be averaged. On the other hand, the Maxwell−Stefan diffusion coefficient is a collective property, so that only one data point per time step is available.

The thermodynamic factor Q is defined as[45]

$$Q = 1 + x_1\left(\frac{\partial \ln \phi_1}{\partial x_1}\right)_{T,P} \quad (8)$$

where ϕ_1 is the fugacity coefficient of the solute.

Q can be calculated using any valid thermodynamic model, such as an equation of state (EoS)[44,45] or through molecular simulation.[40] For thermodynamically ideal binary mixtures, it follows that $Q = 1$ and Fick diffusion coefficient is equal to the Maxwell−Stefan diffusion coefficient.

In this work, we calculated the Maxwell−Stefan and subsequently the Fick diffusion coefficients of mixtures consisted of H_2 or CO molecules dissolved in n-C_{12} and n-C_{28}, respectively, at 473 K. The Maxwell−Stefan diffusivity was estimated from MD calculations using the Einstein relationship (eq 7), while the thermodynamic factor Q was calculated from the SAFT EoS.[13]

3.6. Calculations for the Estimation of the Thermodynamic Factor *Q*. The fugacity coefficient ϕ_1 in eq 8 was calculated from the SAFT EoS. Pure component SAFT parameters were calculated by fitting the model to vapor pressure and saturated liquid density data and are shown in Table 7. For all the mixtures examined, a temperature-independent binary interaction parameter, k_{ij}, was used for the interaction energy. The interaction parameter was fitted to experimental phase equilibrium data and is reported in Table 8. Experimental data and SAFT correlations are shown in Figure 6 for H_2−n-C_{12} and CO−n-C_{12} and in Figure 7 for H_2−n-C_{28} and CO−n-C_{28}. In all cases, SAFT provides accurate correlation of the data. The k_{ij} values fitted to phase equilibrium data were used subsequently to predict Q at the temperature and pressure of interest here.

Zabala et al.[45] provided a simple analysis of the effect of the mixture nonideality using the Flory−Huggins model proposed by Fornasiero et al.[53] According to this analysis, the departure from ideality is the sum of a residual and a combinatorial contribution. This departure is calculated using the activity coefficient, defined as $\gamma_i = \phi_i/\phi_i^*$, where ϕ_i^* is the liquid phase pure component fugacity coefficient. The combinatorial contribution that results in a negative contribution ($\ln \gamma_i < 0$) is due to size differences of the molecules (entropic effect). The residual contribution, on the other hand, results in a positive contribution ($\ln \gamma_i > 0$) and is the result of dispersive interactions (enthalpic effect). Molecules whose sizes are relatively similar often show a positive deviation from the ideality, because the enthalpic interactions have a much larger contribution than the entropic interactions. On the other side, mixtures of small and large molecules show a negative deviation from ideality. Moreover, according to Gibbs−Duhem rule, for mixtures that exhibit a negative deviation from ideal behavior, the thermodynamic factor Q, which is related to the slope of the activity coefficient of a component with its mole fraction, will be larger than 1. On the contrary, when the deviation from ideality is positive the slope is negative and the thermodynamic factor Q will be smaller than 1.

In Figure 8, the Q factor is shown for binary mixtures of H_2 and CO with n-C_{12}, n-C_{16}, and n-C_{28}, respectively, at 473 K as a function of the composition. For both solutes, Q factor increases with the n-alkane chain length, at constant

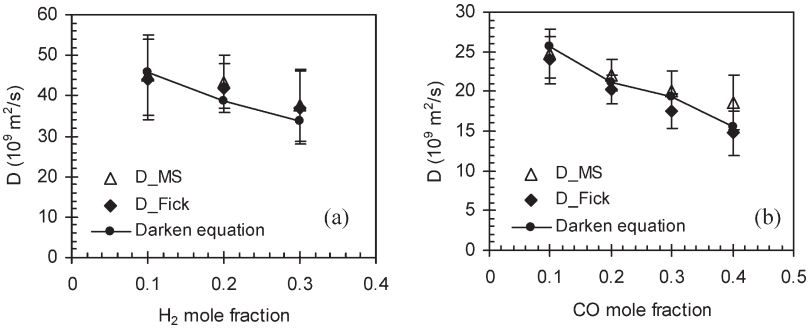

Figure 9. NVT MD predictions for D^{MS} and D^{Fick} and from Darken equation for D^{MS} for (a) H_2-n-C_{12} and (b) $CO-n$-C_{12} mixtures at 473 K as a function of light-component mole fraction.

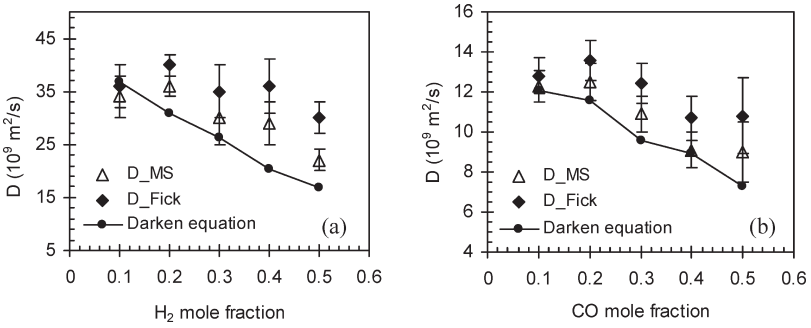

Figure 10. NVT MD predictions for D^{MS} and D^{Fick} and from Darken equation for D^{MS} for (a) H_2-n-C_{28} and (b) $CO-n$-C_{28} mixtures at 473 K as a function of light-component mole fraction.

composition. For the case of H_2 mixtures, Q deviates marginally from 1 for all concentrations for the n-C_{12} mixture while it is higher than 1 for the mixtures with n-C_{16} and n-C_{28}. For the case of CO mixtures, Q is below 1 for the mixtures with n-C_{12} and n-C_{16} and above 1 for the mixture with n-C_{28}. For the latter case, a maximum Q value of 1.2 is observed for CO mole fraction of 0.55. An explanation for this trend may be that, for n-alkanes longer than n-C_{16}, where the size difference of the molecules is higher, the entropic interactions have a larger effect than the enthalpic interactions, and so a negative deviation from the ideality is observed ($Q > 1$). The predictions for Q as a function of composition and n-alkane chain length are very similar to the calculations reported by Zabala et al.[45] for CO_2-n-alkane mixtures.

3.7. Maxwell−Stefan and Fick Diffusion Coefficient Calculations. For the calculation of D^{MS}, NVT MD simulations were performed at different temperature and composition values of each mixture. The density of the mixture was calculated from the SAFT EoS, by selecting a pressure that ensures that the mixture is in the liquid phase and the solute is fully soluble in the n-alkane. In Table 9, the pressure values selected for the various state points for the MD simulations are presented. In all cases, these values are higher than the corresponding phase equilibrium values.

The simulated systems consisted of 60 n-C_{12} or 30 n-C_{28} chain molecules and a number of H_2 or CO molecules to match the composition selected. The duration of the simulation runs was up to 40 ns. To increase the accuracy of the D^{MS} calculations, eight (five for the mixtures with n-C_{28}) different initial structures were examined. However, it can be seen that even after averaging over all runs the standard deviation of the mean value of D^{MS} is still high, especially for the case of H_2 molecules.

In Table 10 and Figures 9 and 10, the simulation results for D^{MS} and D^{Fick} for all mixtures at 473 K are presented. No experimental data were found in the literature for a comparison. For a constant solute concentration, D^{MS} decreases as the n-alkane chain length increases. It is expected that D^{MS} will exhibit an asymptotic behavior with the n-alkane chain length, similar to the one shown for D^{self} in Figure 5.

The binary D^{MS} diffusion coefficient can be estimated from empirical correlations that relate the self-diffusion coefficients or infinite dilution binary diffusion coefficients to the binary D^{MS} as a function of composition.[54−56] In this work, the Darken equation[54] was used. It relates the self-diffusion coefficients of the two components D_1^{self} and D_2^{self} to the binary Maxwell−Stefan diffusion coefficient D_{12}^{MS} through the expression

$$D_{12}^{MS} = D_1^{self} x_2 + D_2^{self} x_1 \quad (9)$$

D^{MS} predictions from the Darken equation are shown in Figures 9 and 10 as lines.

For the H_2-n-C_{12} mixture, the two diffusion coefficients (D^{MS} and D^{Fick}) are very close to each other, given the fact that the Q factor is almost equal to 1. On the other hand, for the $CO-n$-C_{12} mixture, D^{Fick} depends stronger on the CO concentration compared to D^{MS} and this behavior is consistent with the variation of Q with the CO concentration (Figure 8b). Based on the calculations presented in Figure 9, one may conclude that MD predictions for D^{MS} and Darken equation agree remarkably well for the H_2-n-C_{12} and $CO-n$-C_{12} mixtures.

For the case of n-C_{28} mixtures, D^{MS} exhibits a stronger composition dependence compared toD^{Fick}. It is worth noting that, for

dx.doi.org/10.1021/jp1063269 |J. Phys. Chem. B 2011, 115, 1429–1439

$H_2-n\text{-}C_{28}$ and $CO-n\text{-}C_{28}$ mixtures, $D^{Fick} > D^{MS}$, since Q is always greater than 1. Here again, predictions for D^{MS} from Darken equation agree well with MD predictions for the case of $H_2-n\text{-}C_{28}$ and $CO-n\text{-}C_{28}$ mixtures.

4. CONCLUSIONS

In this work, the diffusion of three light components, namely H_2, CO, and H_2O, to heavy *n*-alkanes at elevated temperatures and pressures was examined using MD simulations. Accurate atomistic force fields were used to model *n*-alkane chains and light-component molecules. The force field for the *n*-alkanes was initially validated against experimental density values for different chain lengths and was shown to be very accurate.

The self-diffusion coefficients of the light components to various *n*-alkanes, from $n\text{-}C_{12}$ up to $n\text{-}C_{96}$, were calculated subsequently. Results agreed satisfactorily with limited experimental data for the relatively shorter *n*-alkanes.

Finally, long MD simulations were performed for the estimation of the Maxwell−Stefan and Fick diffusion coefficient of H_2 and CO in $n\text{-}C_{12}$ and $n\text{-}C_{28}$. No experimental data are available in the literature to validate our calculations. For the calculation of the nonideal thermodynamic factor Q to the Fick diffusion coefficient, the SAFT EoS was used with a binary interaction parameter fitted to phase equilibrium data. The factor Q assumed values below, equal to, or even higher than 1, depending on the composition of the binary mixtures. Simulation results for the Maxwell−Stefan diffusion coefficient were compared against the empirical Darken equation and found to be in very good agreement for the case of H_2 and CO diffusing through the hydrocarbons.

AUTHOR INFORMATION

Corresponding Author

*E-mail: economou@chem.demokritos.gr.

ACKNOWLEDGMENT

Financial support from Shell Global Solutions International BV through a contracted research agreement is gratefully acknowledged.

REFERENCES

(1) Kowert, B.; Sobush, K.; Fuqua, C.; Mapes, C.; Jones, J.; Zahm, J. *J. Phys. Chem. A* **2003**, *107*, 4790.
(2) Medvedev, O.; Shapiro, A. *Fluid Phase Equilib.* **2004**, *225*, 13.
(3) Liu, H.; Silva, C. M.; Macedo, E. A. *Fluid Phase Equilib.* **2002**, *202*, 89.
(4) Harmandaris, V. A.; Doxastakis, M.; Mavrantzas, V. G.; Theodorou, D. N. *J. Chem. Phys.* **2002**, *116*, 436.
(5) Harmandaris, V. A.; Angelopoulou, D.; Mavrantzas, V. G.; Theodorou, D. N. *J. Chem. Phys.* **2002**, *116*, 7656.
(6) Krishna, R.; van Baten, J. M. *Ind. Eng. Chem. Res.* **2005**, *44*, 6939.
(7) Dysthe, D. K.; Fuchs, A. H.; Rousseau, B.; Durandeau, M. *J. Chem. Phys.* **1999**, *110*, 4060.
(8) Martin, M. G.; Siepmann, J. I. *J. Phys. Chem. B* **1998**, *102*, 2569.
(9) Berendsen, H. J. C.; Grigera, J. R.; Straatsma, T. P. *J. Phys. Chem.* **1987**, *91*, 6269.
(10) Rodden, J. B.; Erkey, C.; Akgerman, A. *J. Chem. Eng. Data* **1988**, *33*, 450.
(11) Matthews, M. A.; Rodden, J. B.; Akgerman, A. *J. Chem. Eng. Data* **1987**, *32*, 319.
(12) Schatzberg, P. *J. Polym. Sci. Part C* **1965**, *10*, 87.
(13) Huang, S. H.; Radosz, M. *Ind. Eng. Chem. Res.* **1990**, *29*, 2284.
(14) Ferrando, N.; Ungerer, P. *Fluid Phase Equilib.* **2007**, *254*, 211.
(15) Hirschfelder, J. O.; Curtiss, C. F.; Bird, R. B. *Molecular Theory of Gases and Liquids*; Wiley: New York, 1954.
(16) Potoff, J. J.; Panagiotopoulos, A. Z. *J. Chem. Phys.* **1998**, *109*, 10914.
(17) Darkrim, F.; Vermesse, J.; Malbrunot, P.; Levesque, D. *J. Chem. Phys.* **1999**, *110*, 4020.
(18) Cracknell, R. F. *Phys. Chem. Chem. Phys.* **2001**, *3*, 2091.
(19) Nosé, S.; Klein, M. L. *Mol. Phys.* **1983**, *50*, 1055.
(20) Gear, C. W. *Numerical Initial Value Problems in Ordinary Differential Equations*; Prentice-Hall: Englewood Cliffs, NJ, 1971.
(21) Theodorou, D. N.; Suter, U. W. *Macromolecules* **1985**, *18*, 1467.
(22) Theodorou, D. N.; Boone, T. D.; Dodd, L. R.; Mansfield, K. F. *Macromol. Chem., Theory Simul.* **1993**, *2*, 191.
(23) Allen, M. P.; Tildesley, D. J. *Computer Simulation of Liquids*; Oxford Science Publications: Oxford, UK, 1987.
(24) Berendsen, H. J. C.; Postma, J. P. M.; van Gunsteren, W. F.; DiNola, A.; Haak, J. R. *J. Chem. Phys.* **1984**, *81*, 3684.
(25) See: http://webbook.nist.gov.
(26) Daubert, T. E.; Danner, R. P. *Physical and Thermodynamic Properties of Pure Chemicals: Data Compilation*; Hemisphere: New York, 2003.
(27) Poling, B. E.; Prausnitz, J. M.; O'Connell, J. P. *The Properties of Gases and Liquids*, 5th ed.; McGraw-Hill Co.: New York, 2001.
(28) Elbro, H. S.; Fredenslund, A.; Rasmussen, P. *Ind. Eng. Chem. Res.* **1991**, *30*, 2576.
(29) Harmandaris, V. A.; Doxastakis, M.; Mavrantzas, V. G.; Theodorou, D. N. *J. Chem. Phys.* **2002**, *116*, 436.
(30) Dee, G. T.; Ougizawa, T.; Walsh, D. J. *Polymer* **1992**, *33*, 3462.
(31) Zúniga, I.; Bahar, I.; Dodge, R.; Mattice, W. L. *J. Chem. Phys.* **1991**, *95*, 5348.
(32) Zervopoulou, E.; Mavrantzas, V. G.; Theodorou, D. N. *J. Chem. Phys.* **2001**, *115*, 2860.
(33) Zervopoulou, E. Ph.D. Thesis, University of Patras, Greece, 2000.
(34) Mavrantzas, V. G.; Boone, T. D.; Zervopoulou, E.; Theodorou, D. N. *Macromolecules* **1999**, *32*, 5072.
(35) Baschnagel, J.; Qin, K.; Paul, W.; Binder, K. *Macromolecules* **1992**, *25*, 3117.
(36) Brown, D.; Clarke, J. H. R.; Qkuda, M.; Yamazaki, T. *J. Chem. Phys.* **1994**, *100*, 1684.
(37) Modello, M.; Grest, G. S.; Webb, E. B., III; Peczak, P. *J. Chem. Phys.* **1998**, *109*, 798.
(38) Paul, W.; Smith, G. D.; Yoon, D. Y. *Macromolecules* **1997**, *30*, 7772.
(39) Hoheisel, C. *Phys. Rep.* **1994**, *245*, 111.
(40) Zhou, Z.; Todd, B. D.; Travis, K. P.; Sadus, R. J. *J. Chem. Phys.* **2005**, *123*, 054505.
(41) Fernández, G. A.; Vrabec, J.; Hasse, H. *Int. J. Thermophys.* **2004**, *25*, 175.
(42) Zhang, L.; Liu, Y.-Ch; Wang, Q. *J. Chem. Phys.* **2005**, *123*, 144701.
(43) Krishna, R.; van Baten, J. M. *Ind. Eng. Chem. Res.* **2005**, *44*, 6939.
(44) Zhang, L.; Wang, Q.; Liu, Y.-Ch; Zhang, L.-Zh *J. Chem. Phys.* **2006**, *125*, 104502.
(45) Zabala, D.; Nieto-Draghi, C.; de Hemptinne, J.Ch.; López de Ramos, A. L. *J. Phys. Chem. B* **2008**, *112*, 16610.
(46) Dysthe, D. K.; Fuchs, A. H.; Rousseau, B. *Int. J. Thermophys.* **1998**, *19*, 437.
(47) Jolly, D. L.; Bearman, R. J. *Mol. Phys.* **1980**, *41*, 137.
(48) Schoen, M.; Hoheisel, C. *Mol. Phys.* **1984**, *52*, 33.
(49) Gao, W.; Robinson, R. L.; Gasem, K. A. M. *J. Chem. Eng. Data* **1999**, *44*, 130.
(50) Florusse, L. J.; Peters, C. J.; Pàmies, J. C.; Vega, L. F.; Meijer, H. *AIChE* **2003**, *49*, 3260.
(51) Park, J.; Robinson, R. L., Jr.; Gasem, K. A. M. *J. Chem. Eng. Data* **1995**, *40*, 241.

(52) Srivatsan, S.; Yi, X.; Robinson, R. L., Jr.; Gasem, K. A. M. *J. Chem. Eng. Data* **1995**, *40*, 237.
(53) Fornasiero, F.; Prausnitz, J.; Radke, J. *Macromolecules* **2005**, *38*, 1364.
(54) Darken, L. S. *Trans. Am. Inst. Mining Metall. Eng.* **1948**, *175*, 184.
(55) Caldwell, C. S.; Babb, A. L. *J. Phys. Chem.* **1956**, *60*, 51.
(56) Vignes, A. *Ind. Eng. Chem. Fundam.* **1966**, *5*, 189.